Work function modulation in MgO/Nb:$SrTiO_3$ by utilizing highly nonequilibrium thin-film growth

Tomofumi Susaki,* Nobuhiro Shigaki, Kosuke Matsuzaki, and Hideo Hosono†

Secure Materials Center, Materials and Structures Laboratory, Tokyo Institute of Technology, Nagatsuta, Midori, Yokohama 226-8503, Japan

(Received 2 June 2014; revised manuscript received 21 July 2014; published 31 July 2014)

We have controlled the amount of charged defects in MgO thin films grown on Nb-doped $SrTiO_3$ (Nb:$SrTiO_3$) substrate by pulsed laser deposition at room temperature. The work function of MgO/Nb:$SrTiO_3$ varies from ∼2 to ∼5 eV depending on the partial oxygen pressure during film growth. The increase in the work function under the oxygen-rich deposition condition is consistent with the dipole moment formation at the interface, which is given by negatively charged V^- centers in MgO thin films and the corresponding image charges in the conductive substrate. That the formation of charged defects in an insulating capping layer can induce a strong modulation of work function as large as ∼3 eV implies that controlling charged defects could be an effective method to design the electronic properties of oxide surfaces.

DOI: 10.1103/PhysRevB.90.035453 PACS number(s): 73.30.+y, 73.20.−r, 68.55.Ln

I. INTRODUCTION

When heterointerfaces are formed between two materials, new electronic states and resulting physical properties, which are not found in either of the ingredients, can emerge, giving rise to various electronic [1] and catalytic functionalities [2]. In Schottky junctions, the metal and semiconductor are joined to give an insulating depletion layer at the interface, where the work function of the metal plays a key role in determining the qualitative characteristics of the interface [1]. The metal-insulator interface is another indispensable ingredient to design artificial electronic states: Controlling the metal-insulator interface has indeed been central in modern condensed-matter physics and electronic device fabrication. In order to understand the electronic states and functionalities in metal-insulator heterostructures, a metal surface covered with an insulating thin film has been used as a model system, which is free from charging up during spectroscopic measurements [2].

Recently, a tunable work function at metal-insulator interfaces has been attracting considerable attention [3–14] since such a work-function modulation is induced by an interplay of various physical and chemical effects characteristic of the metal-insulator interface and since it is directly relevant for developing new catalytic and electronic activity at solid surfaces. Interface effects contributing to a change in the work function include (i) the electron compression effect [3–9], where leaked free electrons at a bare metal surface are pushed back by the hard-wall-type potential of insulating layer, (ii) electron transfer between a metal and an insulator [4,5], (iii) rumpling of cation and anion layers in the surface of insulator [13], (iv) dipole moment formation in the insulating layer itself along the surface normal direction [10], and (v) the effect of charged point defects in the insulating layer [11]. All of these effects modulate the existing dipole moment at the metal surface or create a new dipole moment at the interface, modulating the effective work function. Recent first-principles calculations [3–5,11–13] and work-function measurements [6–10,14], represented by a Kelvin probe microscopy study, have revealed that the surface work function of metal is indeed strongly modulated by depositing thin insulating films.

In this paper we report that in addition to the electron compression effect, charged defects in MgO, which can be introduced to the near interface region by a highly nonequilibrium film growth technique, induce a significant modulation of the effective work function in MgO/Nb:$SrTiO_3$: The sign of work-function modulation switches depending on the film growth condition and the extent of modulation is as large as ∼3 eV. This result indicates that charged defects in MgO, which can obviously contribute to the interface dipole and hence the effective work function, can be stabilized due to image charges and lattice distortion, both of which are characteristic of the metal-insulator heterointerface. Such mechanisms intrinsic to interfaces would become more and more important to further develop functionalities at heterostructures as the dimension of the system is further scaled down.

II. EXPERIMENT

TiO_2-terminated conductive $SrTiO_3$(100) substrates doped with 0.5 wt. % Nb (Nb:$SrTiO_3$) and etched with buffered NH_4F-HF solutions [15] were annealed at 740 °C for 20 min in the deposition chamber. The oxygen partial pressure $p(O_2)$ during annealing was the same as that during deposition. To grow MgO films by pulsed laser deposition, we used a single crystalline MgO target and a KrF excimer laser with an energy of ∼100 mJ incident to the deposition chamber and a repetition rate of 10 Hz. After a small amount of MgO was deposited, samples were transferred to the measurement chamber, where the work function was measured by the Kelvin probe technique (KP Technology) with the counterelectrode of a 4-mm ϕ stainless-steel plate, which was oscillated with a frequency of 66 Hz, without exposing the sample surface to air. We applied an offset voltage between the counterelectrode and Nb:$SrTiO_3$ substrate: The offset voltage plus the difference in the vacuum level between the counterelectrode and sample gives an electric field, which depends on the distance of the gap space. Such an electric field then induces charges in both the counterelectrode and the sample. As the counterelectrode vibrates, the gap distance oscillates and hence the

*susaki@msl.titech.ac.jp

†Also at Frontier Research Center, Tokyo Institute of Technology, Nagatsuta, Midori, Yokohama 226-8503, Japan and Materials and Structures Laboratory, Tokyo Institute of Technology, Nagatsuta, Midori, Yokohama 226-8503, Japan.

amount of charge in the counterelectrode oscillates, giving an alternating current (Kelvin probe signal). One can measure the work function of the sample with respect to that of the counterelectrode by monitoring the offset voltage dependence of the Kelvin probe signal. The value of the work function was calibrated by defining the value of evaporated gold to be 5.1 eV [16]. When MgO films were deposited at 700 °C, samples were transferred to the measurement chamber after the samples were cooled to ∼100 °C. Oxygen was not introduced to the measurement chamber, where the pressure was below 1×10^{-6} Pa. A typical deposition rate was 0.04–0.06 nm/s, which was determined by x-ray-reflection (XRR) measurement [17]. We repeated a cycle of deposition and work-function measurements more than 10 times under each deposition condition. The samples were further characterized by atomic force microscopy (AFM) and x-ray diffraction (XRD).

III. RESULTS

The work function of MgO/Nb:$SrTiO_3$ deposited at 700 °C and room temperature with $p(O_2)$ varied from 1×10^{-7} to $1 \times 10^{+1}$ Pa is shown in Figs. 1(a) and 1(b) as a function of MgO thickness. We have found that the Kelvin probe signal, which was a sinelike wave corresponding to the vibration of the counterelectrode, is almost independent of the MgO thickness up to ∼100 nm. However, since some of the work-function values are scattered as the MgO thickness exceeds ∼50 nm, here we plot the work function up to ∼30 nm.

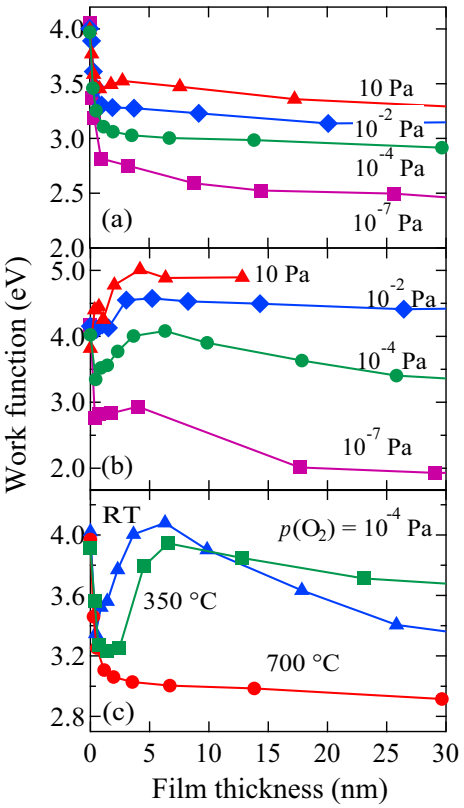

FIG. 1. (Color online) Work function of MgO/Nb:$SrTiO_3$ as a function of MgO thickness deposited at (a) 700 °C and (b) room temperature (RT). Here $p(O_2)$ was 10 Pa (triangles), 10^{-2} Pa (diamonds), 10^{-4} Pa (circles), and 10^{-7} Pa (squares). (c) Work function of MgO/Nb:$SrTiO_3$ deposited under $p(O_2) = 10^{-4}$ Pa at 700 °C (circles), 350 °C (squares), and RT (triangles).

The work function of bare Nb:$SrTiO_3$ substrate is ∼4.0 eV, which is slightly lower than reported values [18,19]. The difference from the values [9,10] measured by the same technique would be due to the improved vacuum condition in the measurement chamber. As MgO is deposited at 700 °C [Fig. 1(a)], the work function sharply drops up to 1 nm and is almost independent of the thickness beyond that. The extent of the work-function reduction is enhanced as $p(O_2)$ decreases from 10 to 10^{-7} Pa. These characteristics are qualitatively similar to those observed in MgO/Nb:$SrTiO_3$ deposited at 740 °C [9]. A sharp reduction of the work function with MgO deposition is consistent with the electron compression model, where the leaked electrons are pushed back by the hard-wall-type potential of MgO. That the thickness dependence of the work function is weak beyond 1 nm indicates that the MgO films grown at 700 °C contain little charges responding to the oscillating counterelectrode. While the oxygen pressure dependence was not observed between $p(O_2) = 10^{-1}$ and 10^{-3} Pa in previous work [9], the present result clearly shows a further reduction in the work function with decreasing $p(O_2)$ from 10^{-2} to 10^{-7} Pa, again suggesting the improved vacuum condition in the measurement chamber.

The MgO thickness dependence and $p(O_2)$ dependence of the work function of MgO/Nb:$SrTiO_3$ deposited at room temperature are, however, very different from those deposited at 700 °C. As shown in Fig. 1(b), while the work function decreases with initial deposition under the oxygen-poor condition as in $p(O_2) = 10^{-7}$ Pa, the work function increases and shows a broad maximum at ∼5 nm under the oxygen-rich condition. Since the work function should decrease as an insulating layer is deposited according to the electron compression model, the present observation of an increase in the work function with MgO deposition indicates that a different mechanism dominates the characteristics of MgO/Nb:$SrTiO_3$ deposited under the oxygen-rich condition at room temperature.

We compare the work function of MgO/Nb:$SrTiO_3$ deposited at various temperatures with $p(O_2) = 10^{-4}$ Pa in Fig. 1(c). The sharp drop of the work function with initial deposition, which dominates the characteristics of the 700 °C sample, is also partially present in 350 °C and RT samples. On the other hand, the broad maximum around ∼5 nm evolves in going from 350 °C to room temperature. The length scale is clearly different between the sharp drop at the interface and the broad maximum formation.

In Fig. 2 we show the topographic AFM images of the sample surface with the film thickness of ∼20 nm. The terrace and step structure is present more clearly in the films deposited at room temperature as shown in Figs. 2(e)–2(g). Since the observed terrace width agrees with a typical terrace width of Nb:$SrTiO_3$(100) substrate, we believe that the clearer edge structure in the film deposited at room temperature just replicates the substrate surface morphology due to the smaller grain size and to lower film crystallinity as observed in BeO films grown on $SrTiO_3$ [20]. The root-mean-square surface roughness is as small as a few angstroms and is almost the same between 700 °C and room-temperature deposition as shown in Fig. 2(h), suggesting that the surface roughness

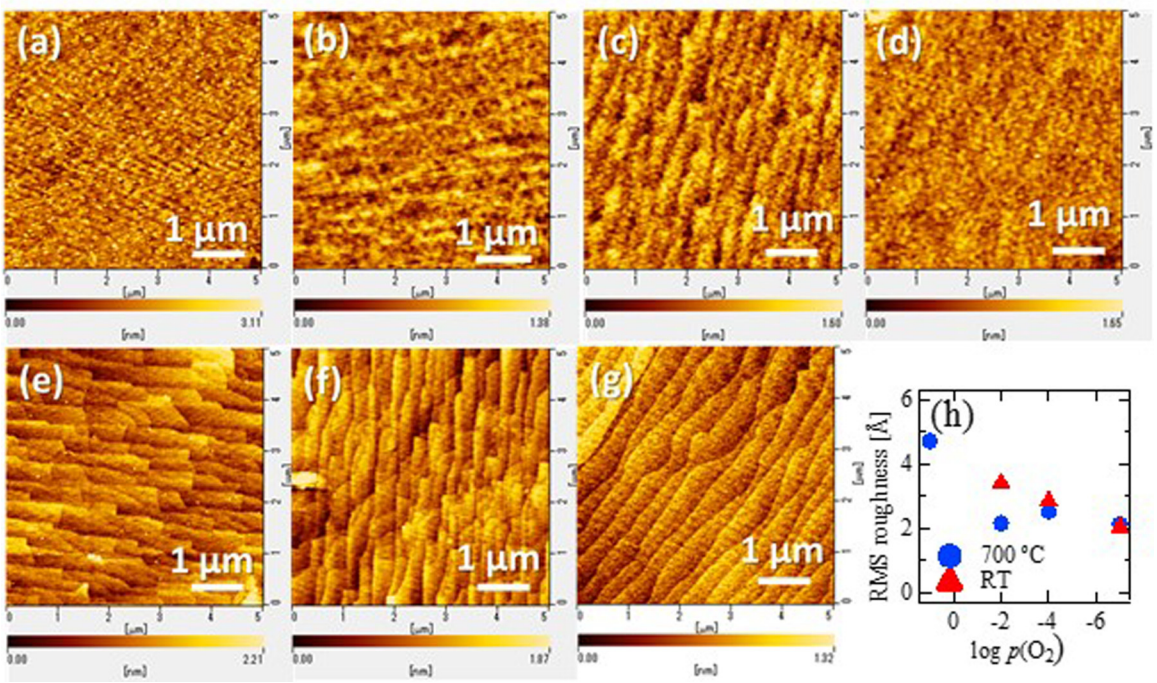

FIG. 2. (Color online) Topographic images measured by AFM for ~20-nm-thick MgO films deposited on Nb:SrTiO$_3$ at (a) 700 °C and $p(O_2) = 10$ Pa, (b) 700 °C and $p(O_2) = 10^{-2}$ Pa, (c) 700 °C and $p(O_2) = 10^{-4}$ Pa, (d) 700 °C and $p(O_2) = 10^{-7}$ Pa, (e) RT and $p(O_2) = 10^{-2}$ Pa, (f) RT and $p(O_2) = 10^{-4}$ Pa, and (g) RT and $p(O_2) = 10^{-7}$ Pa. (h) Root-mean-square surface roughness plotted as a function of $p(O_2)$.

including the interface roughness, which could contribute to the work-function modulation in general [21], does not play a dominant role in the present case.

Figure 3 shows an out-of-plane XRD pattern of MgO films deposited on Nb:SrTiO$_3$ at various temperatures with $p(O_2) = 10^{-4}$ Pa. All the films are completely (100) oriented, where no signal corresponding to the (110) or (111) orientation is present. While the peak position of the MgO film deposited at 700 °C agrees with that of bulk MgO, the peak position shifts to the lower angle side with the peak width increased as the deposition temperature decreases. A wider XRD peak in the film deposited at room temperature indicates the smaller grain size and lower film crystallinity, consistent with the observation by AFM.

The lattice constant of MgO films deposited at room temperature was further studied by high-resolution XRD measurement as shown in Fig. 4. The lattice constant is larger along

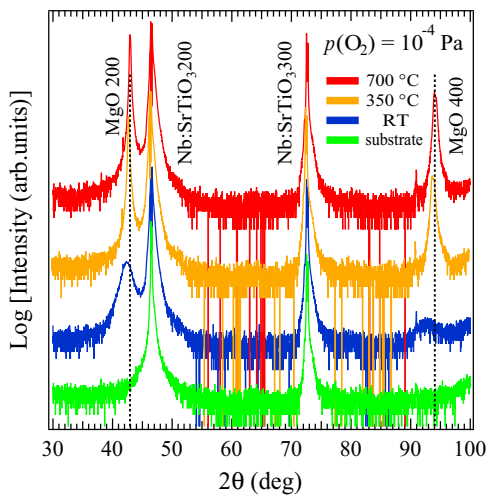

FIG. 3. (Color online) Out-of-plane x-ray-diffraction pattern of MgO films deposited on Nb:SrTiO$_3$ with that of bare Nb:SrTiO$_3$ substrate. The film thickness is 110–150 nm. The dotted lines indicate the peak position corresponding to the bulk lattice constant of MgO (4.211 Å).

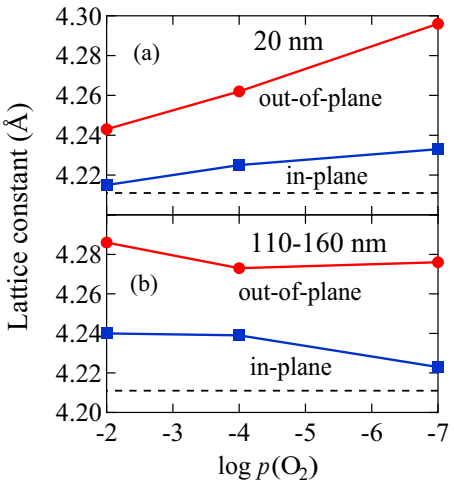

FIG. 4. (Color online) Out-of-plane (circles) and in-plane (squares) lattice constant of MgO films deposited on Nb:SrTiO$_3$ at RT as a function of $p(O_2)$. The film thickness is (a) ~20 nm and (b) 110–160 nm. The (110–160)-nm-thick samples were those used for thickness-dependent work-function measurements [Fig. 1(b)] and hence the growth was interrupted more than ten times. The bulk value of 4.211 Å is indicated by dashed lines.

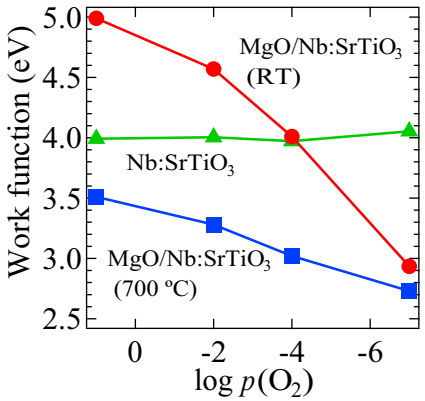

FIG. 5. (Color online) Work function of MgO/Nb:$SrTiO_3$ at the film thickness of 4 nm as a function of of $p(O_2)$. The work function is plotted by circles for RT deposition and squares for 700 °C deposition. The work function of Nb:$SrTiO_3$ substrate before depositing MgO is also plotted by triangles.

the out-of-plane direction than the in-plane direction. Although the lattice constant of Nb:$SrTiO_3$ is ~7% smaller than that of MgO, the in-plane lattice constant is still larger than the bulk value in the present films deposited at room temperature, while that of MgO thin films deposited at high temperatures is smaller than the bulk value [9,22], indicating that the interface strain is weaker in room-temperature deposited films. As the deposition condition becomes oxygen rich, i.e., from $p(O_2) = 10^{-7}$ to 10^{-2} Pa, the lattice volume slightly increases in (110–160)-nm-thick films, while it is systematically reduced in 20-nm-thick films.

In Fig. 5 we show the $p(O_2)$ dependence of the work function of MgO/Nb:$SrTiO_3$ at 4-nm thickness prepared at 700 °C and room temperature as well as that of bare Nb:$SrTiO_3$ substrate. The work function of bare Nb:$SrTiO_3$ does not depend on $p(O_2)$ at all. While performed at 700 °C, MgO deposition lowered the work function and the extent of the work-function reduction increased in going from the oxygen-rich [$p(O_2) = 10^{+1}$ Pa] to the oxygen-poor [$p(O_2) = 10^{-7}$ Pa] condition, as observed in MgO/Nb:$SrTiO_3$ deposited at 740 °C [9]. On the other hand, with MgO deposition at room temperature, the work function decreased under the oxygen-poor condition, while it increased under the oxygen-rich condition.

IV. DISCUSSION

While pure MgO is optically transparent reflecting the large band gap of 7.8 eV [23], the formation of point defects can color the crystal [24–33]. Such color centers in MgO are classified into oxygen vacancies (F centers) and magnesium vacancies (V centers). A removal of O^{2-} gives doubly positively charged vacancies (F^{2+} centers), which are transformed to singly charged (F^+ centers) and neutral vacancies (F centers) by trapping one and two electrons, respectively. Similarly, doubly negatively charged magnesium vacancies (V^{2-} centers) are transformed to V^- and V centers with one and two holes trapped, respectively. While the MgO lattice is very stable and hence does not accommodate many point defects under the equilibrium condition [24–26], x-ray or γ-ray [27], electron [28], and neutron [28–30] irradiation or high-temperature annealing [31] can increase the defect concentration. Here, since the local atomic structure is strongly modified at such point defects [30], at the surfaces where the ions are low coordinated, various point defects are formed and stabilized more easily [24,33], playing key roles in the catalytic activities of MgO. This is also true at the interface: A deviation from the rigid bulk structure can be favorable for the formation of point defects. In addition, in the case of the interface between MgO and metal, charged point defects such as F^+ or V^- centers can be further formed and stabilized due to the presence of a charge reservoir and by the formation of image charges [34]. The presence of charged point defects in MgO and the corresponding image charges in metal induces the dipole moment at the metal-MgO interface, modulating the effective work function. Indeed, recent density functional theory calculations show that the work function of the MgO/metal system can increase or decrease by introducing charged impurities to the MgO layer [11].

In Fig. 6 we schematically show how the work function of the metal surface can be modified by depositing an insulating layer with and without such charged defects. As demonstrated by many theoretical and experimental studies, depositing an insulating layer on metal substrate suppresses the amount of electrons that are leaked away from the immobile framework of cations, reducing the dipole moment and hence the work function [Figs. 6(a) and 6(b)] [3–9]. When negatively charged defects such as V^- centers are introduced to the insulating layer, the electrons of the near interface region are further pushed away from the interface with increased positive charges of the cation framework playing the role of the increased image charges, where the increased dipole moment gives a larger work function [Fig. 6(c)] [11]. On the other hand, positively charged defects such as F^+ centers would pull the electrons of

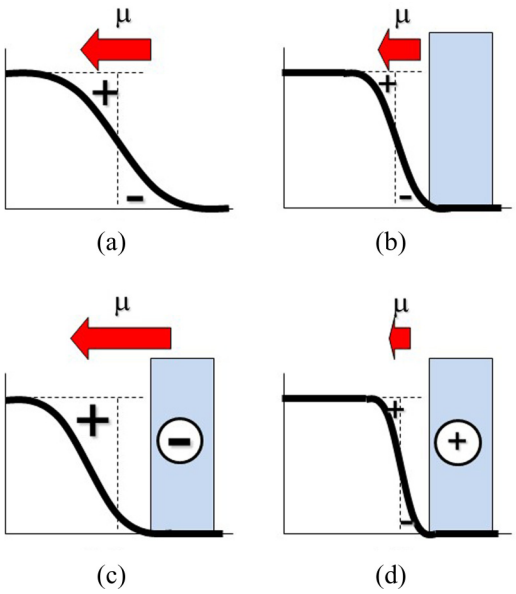

FIG. 6. (Color online) Schematic electron distribution profile and the surface dipole moment μ at (a) the bare metal surface and at the metal surface covered with (b) neutral, (c) negatively charged, and (d) positively charged insulating layers.

the metal to the interface, reducing the dipole moment and the work function [Fig. 6(d)].

Here, as the deposition temperature decreases, one can expect to quench a highly nonequilibrium phase in the films grown by pulsed laser deposition. A systematic change in the work function as a function of $p(O_2)$ shown in Fig. 5, which is weakly present in 700 °C deposited samples and is significantly present in room-temperature deposited samples, would indicate that defect formation depending on the deposition condition dominates the work-function modulation. Also, since the work function of any ingredient of the present structure is smaller than 5 eV, namely, 2.7–4.4 eV (MgO) [35,36], 3.66 eV (Mg) [37], and 4.1–4.3 eV ($SrTiO_3$) [18,19], the work function of room-temperature prepared MgO/Nb:$SrTiO_3$ deposited under the oxygen-rich condition as high as ∼5 eV would reflect a dominant contribution of negatively charged magnesium vacancies near the interface. Since the formation energy of V^- centers is smaller than that of V^{2-} centers [25], we think that V^- centers rather than V^{2-} centers dominate the work function of room-temperature prepared samples. On the other hand, the work function of MgO/Nb:$SrTiO_3$ deposited under the oxygen-poor condition does not depend on the deposition temperature very much in spite of the large lattice expansion revealed in Fig. 4, which would suggest the presence of a finite number of oxygen vacancies [29]. This behavior is consistent with a calculated result for MgO/Mo with positively charged impurities included in the MgO layer: Even when the MgO layer is neutral, the work function of the MgO/Mo interface is already as low as ∼2 eV due to the strong electron compression effect and thus it cannot be further reduced by introducing positively charged impurities to MgO [11].

In Fig. 1 we have shown that a broad maximum appears at ∼5 nm under the oxygen-rich condition in the work function versus film thickness plot. As we have already mentioned, a deviation from the bulk crystal structure as well as the presence of a charge reservoir and hence the formation of image charges would contribute to the formation of many charged defects in the interfacial region of MgO. However, when the position of the charged defects is too close to the conducting substrate, such charged defects would easily be neutralized by tunneled electrons from or to the substrate. The observed broad maximum would indicate that V^- centers are stable when placed away from the interface by around 5 nm.

We have pointed out that the lattice constant in 20-nm-thick films systematically depends on $p(O_2)$, in contrast to the behavior observed in (110–160)-nm-thick films (Fig. 5). Although the length scale of the XRD study is much larger than that of work-function modulation, such a position dependence of the deviation from the bulk crystal structure would partly correspond to the strong thickness dependence of the work function. Direct measurements of defect concentrations as well as their spatial profile would be an important future work to further understand and control the present interface. An electroluminescence study combined with a scanning tunneling microscope might give useful information [38,39]. A gradual work-function decrease with further deposition beyond 5 nm should also be clarified in the future.

V. CONCLUSION

By introducing charged defects such as V^- centers in MgO, we have further controlled the interface dipole moment and hence the work function of MgO/Nb:$SrTiO_3$, where the electron compression effect also contributes to the work function regardless of the presence of such charged defects. The formation of the interfacial layer in MgO with a large number of charged defects is due to a deviation from the rigid bulk crystal structure at the interface and to the presence of image charges induced in Nb:$SrTiO_3$, both of which are intrinsic to metal-insulator heterointerfaces. These effects rely on the fact that MgO is robustly insulating against chemical doping; i.e., the MgO layer near the interface in the present system is still insulating even after many charged defects are introduced. The present finding of work-function modulation by ∼3 eV demonstrates that the insulator/metal system, combined with the formation of charged defects in the insulating layer, shows great controllability in the surface electronic properties.

ACKNOWLEDGMENTS

This work was financially supported by JSPS KAKENHI Grant No. 25286056 and by Ministry of Education, Culture, Sports, Science and Technology, Japan (Elements Strategy Initiative to Form Core Research Center).

[1] S. M. Sze, *Physics of Semiconductor Devices*, 2nd ed. (Wiley, New York, 1981).
[2] H.-J. Freund and G. Pacchioni, Chem. Soc. Rev. **37**, 2224 (2008).
[3] J. Goniakowski and C. Noguera, Interface Sci. **12**, 93 (2004).
[4] L. Giordano, F. Cinquini, and G. Pacchioni, Phys. Rev. B **73**, 045414 (2006).
[5] S. Prada, U. Martinez, and G. Pacchioni, Phys. Rev. B **78**, 235423 (2008).
[6] T. König, G. H. Simon, H.-P. Rust, and M. Heyde, J. Phys. Chem. C **113**, 11301 (2009).
[7] M. E. Vaida, T. Gleitsmann, R. Tchitnga, and T. M. Bernhardt, J. Phys. Chem. C **113**, 10264 (2009).
[8] M. Bieletzki, T. Hynninen, T. M. Soini, M. Pivetta, C. R. Henry, A. S. Foster, F. Esch, C. Barth, and U. Heiza, Phys. Chem. Chem. Phys. **12**, 3203 (2010).
[9] T. Susaki, A. Makishima, and H. Hosono, Phys. Rev. B **83**, 115435 (2011).
[10] T. Susaki, A. Makishima, and H. Hosono, Phys. Rev. B **84**, 115456 (2011).
[11] S. Prada, L. Giordano, and G. Pacchioni, J. Phys. Chem. C **116**, 5781 (2012).
[12] S. B. Cho, K.-H. Yun, D. S. Yoo, K. Ahn, and Y.-C. Chung, Thin Solid Films **544**, 541 (2013).
[13] S. Ling, M. B. Watkins, and A. L. Shluger, Phys. Chem. Chem. Phys. **15**, 19615 (2013).

[14] T. Susaki and H. Hosono, Jpn. J. Appl. Phys. **52**, 110125 (2013).
[15] M. Kawasaki, K. Takahashi, T. Maeda, R. Tsuchiya, M. Shinohara, O. Ishiyama, T. Yonezawa, M. Yoshimoto, and H. Koinuma, Science **266**, 1540 (1994).
[16] D. E. Eastman, Phys. Rev. B **2**, 1 (1970).
[17] An XRR fringe pattern corresponding to the film thickness was not observed for the MgO film step-by-step deposited on Nb:$SrTiO_3$ at room temperature and $p(O_2) = 10$ Pa [triangles in Fig. 1(b)]. We calibrated the film thickness with the deposition rate based on XRR measurement of MgO thin film deposited under the same condition on a glass plate.
[18] Y. W. Chung and W. B. Weissbard, Phys. Rev. B **20**, 3456 (1979).
[19] L. F. Zagonel, M. Baeurer, A. Bailly, O. Renault, M. J. Hoffmann, S.-J. Shih, and N. Barrett, J. Phys.: Condens. Matter **21**, 314013 (2009).
[20] T. Peltier, R. Takahashi, and M. Lippmaa, Appl. Phys. Lett. **104**, 231608 (2014).
[21] W. Li and D. Y. Li, J. Chem. Phys. **122**, 064708 (2005).
[22] K. Matsuzaki, H. Takagi, H. Hosono, and T. Susaki, Phys. Rev. B **84**, 235448 (2011).
[23] D. M. Roessler and W. C. Walker, Phys. Rev. **159**, 733 (1967).
[24] V. E. Henrich and P. A. Cox, *The Surface Science of Metal Oxides* (Cambridge University Press, Cambridge, 1994).
[25] A. Gibson, R. Haydock, and J. P. LaFemina, Phys. Rev. B **50**, 2582 (1994).
[26] G. Pacchioni and H. Freund, Chem. Rev. **113**, 4035 (2013).
[27] M. M. Abraham, Y. Chen, and W. P. Unruh, Phys. Rev. B **9**, 1842 (1974).
[28] Y. Chen, J. L. Kolopus, and W. A. Sibley, Phys. Rev. **186**, 865 (1969).
[29] B. Henderson and D. H. Bowen, J. Phys. C **4**, 1487 (1971).
[30] L. E. Halliburton, D. L. Cowan, and L. V. Holroyd, Phys. Rev. B **12**, 3408 (1975).
[31] L. A. Kappers, R. L. Kroes, and E. B. Hensley, Phys. Rev. B **1**, 4151 (1970).
[32] M. J. Norgett, A. M. Stoneham, and A. P. Pathak, J. Phys. C **10**, 555 (1977).
[33] A. M. Ferrari and G. Pacchioni, J. Phys. Chem. **99**, 17010 (1995).
[34] L. Giordano, U. Martinez, and G. Pacchioni, J. Phys. Chem. C **112**, 3857 (2008).
[35] V. S. Fomenko, in *Handbook of Thermionic Properties*, edited by G. V. Samsonov (Plenum, New York, 1966).
[36] L. N. Kantorovich, A. L. Shluger, P. V. Sushko, J. Günster, P. Stracke, D. W. Goodman, and V. Kempter, Faraday Discuss. **114**, 173 (1999).
[37] H. B. Michaelson, J. Appl. Phys. **48**, 4729 (1977).
[38] H. M. Benia, X. Lin, H.-J. Gao, N. Nilius, and H.-J. Freund, J. Phys. Chem. C **111**, 10528 (2007).
[39] F. Stavale, N. Nilius, and H.-J. Freund, J. Phys. Chem. Lett. **4**, 3972 (2013).